Sudden Cessation of Katabatic Winds in Adélie Land, Antarctica

HUBERT GALLÉE

Institut d'Astronomie et de Géophysique G. Lemaître, Université Catholique de Louvain, Louvain-la-Neuve, Belgium

PAUL PETTRÉ

Centre National de la Recherche Météorologique, Toulouse, France

GUY SCHAYES

Institut d'Astronomie et de Géophysique G. Lemaître, Université Catholique de Louvain, Louvain-la-Neuve, Belgium

(Manuscript received 8 May 1995, in final form 11 December 1995)

ABSTRACT

The evolution of summer katabatic wind events over the steep slopes of Adélie Land is examined, with emphasis on the sudden cessation of these events. Different idealized large-scale forcings are considered, including a situation that comes very close to one observed during the IAGO (Interaction Atmosphère Glace Océan) campaign, held in the region in November–December 1985. The hydrostatic meso-γ-scale atmospheric model MAR (Modèle Atmosphérique Régional) is used to assess the sensitivity of the simulated cessation process to a prescribed large-scale forcing.

1. Introduction

The katabatic wind is a gravity-driven atmospheric current, which is forced by the cooling of air adjacent to a sloped surface. It is observed all around the world and is called glacier or gravity wind (Mather and Miller 1967). It is generally classified as a mesoscale phenomenon. Over huge ice sheets, such as those covering Antarctica and Greenland, the surface cooling conditions are sufficient for the production of a strong sloped inversion and the subsequent development of intense katabatic winds. In Adélie Land, for example, the coastal zone is one of the most windy regions in the world mainly because of the strength and the regularity of the katabatic winds that blow there throughout the year (Schwerdtfeger 1984).

A rather spectacular phenomenon that is often associated with katabatic wind events is the sudden onset and decay of these winds. This is observed in Adélie Land and other parts of the Antarctic coastal zone. Furthermore, the sudden wind transition is accompanied by a sudden pressure change. This process has been referred to as the "Loewe's phenomenon," or the "katabatic jump," or even simply the "jump." Observations of sudden transitions have been mentioned previously [see, e.g., Ball (1956) and Lied (1964)]. The latter author estimated that the horizontal extent of the Loewe's phenomenon ranges between 50 and 100 m. Some cases have been well documented during the IAGO (Interaction Atmosphère Glace Océan) campaign, held in November–December 1985 (Pettré and André 1991). The katabatic wind cessation process may be of particular importance since it governs further propagation of the cold katabatic air over the ocean and consequently impacts the heat exchanges between the Antarctic ice sheet and the surrounding atmosphere and ocean. Moreover, safety considerations for airplanes and landing strips in the Antarctic coastal zone require that we increase our knowledge of katabatic wind and katabatic wind cessation.

The objective of this paper is to present idealized simulations of katabatic winds in the Adélie Land coastal zone. The sudden katabatic wind cessation observed there on 3 December 1985 will be considered with more attention. Summer conditions are assumed. The two-dimensional version of the hydrostatic primitive equation model MAR (Modèle Atmosphérique Régional) is used. This model was developed from an initial dry version provided by P. Alpert and J. Neumann in 1980 (see Alpert et al. 1982 for a description of this version). Rather than representing accurately all the characteristics of the sudden cessation process, which requires in particular a very small horizontal grid size and the relaxation of the hydrostatic assumption, this paper focuses on the possible hydrostatic causes of this process.

Corresponding author address: Dr. Hubert Gallée, Universite Catholique de Louvain, Institut d'Astronomie et de Géophysique G. Lemaître, Chemin du Cyclotron 2, Louvain-la-Neuve B-1348 Belgium.

TABLE 1. The integration domain. Characteristics of weather station DDU and automatic weather stations D10, D47, and D57.

Station	Latitude, longitude	Distance from coast (km)	Location altitude (m MSL)	Slope	Azimuth of maximum upslope	Grid point: Distance from coast (km)	Grid point: Altitude (m MSL)
DDU	66°40′S, 139°50′E	−5	43	0	210°	−5	0
D10	66°42′S, 139°48′E	5	240	2×10^{-2}	210°	5	246
D47	67°23′S, 138°43′E	110	1560	5.5×10^{-3}	210°	109	1586
D57	68°11′S, 137°32′E	210	2103	6.5×10^{-3}	210°	209	2143

2. The model

The atmospheric model MAR is fully described in Gallée and Schayes (1994) and Gallée (1995). It is a hydrostatic primitive equation model in which the vertical coordinate is the normalized pressure $\sigma = (p - p_t)(p_s - p_t)^{-1}$ (p, p_t = const, and p_s being the pressure, the model-top pressure, and the surface pressure, respectively). The full continuity equation is taken into account. The vertical subgrid-scale fluxes are treated using the $E-\epsilon$ model of turbulence (Duynkerke 1988), allowing the turbulent mixing length to be represented as a function of the local flow characteristics. This is important because of the complex structure of the katabatic layer (Pettré and André 1991; Gallée and Schayes 1992). Detailed solar and longwave radiation schemes are used. The solar radiation scheme is that of Tricot and Berger (1988) modified by Gallée et al. (1991). The longwave radiation scheme follows a wideband formulation of the radiative transfer equation (Morcrette 1984) and was designed for use in general circulation models.

The lateral boundary conditions allow the large-scale motions to be taken into account and involve "relaxing" the model-predicted variables toward their large-scale values (Anthes et al. 1989).

To minimize reflection from the upper boundary, a viscous damping layer is used at the top of the domain. It is similar to that used by Klemp and Lilly (1978) to absorb vertically propagating waves [for more details, see Gallée and Schayes (1994)].

Continental ice is assumed to be covered with snow. In this area the atmospheric model is coupled to the snow model adopting the force–restore modeling formulation for soil, following Deardorff (1978). The soil surface parameters are replaced by those of snow, with an assumed snow densitity of 330 kg m^{-3}. The snow albedo is parameterized by adaptating the relation of Segal et al. (1991):

$$\alpha = \alpha_0 + 0.32 \frac{1}{b}\left(\frac{b+1}{1+2b\cos\theta_z} - 1\right), \quad (1)$$

where $\alpha \leqslant 99\%$ is the snow surface albedo, $\alpha_0 = 80\%$, $b = 2$, and θ_z is the solar zenith angle. The second term of the above expression is set equal to zero for $\theta_z \leqslant 60°$.

The ocean is assumed to be ice-free. The sea surface temperature is prescribed as the freezing point for sea water (271.2 K).

In order to reasonably allow a constant large-scale forcing, the model domain is not too large. It covers the coastal zone of Adélie Land from a distance of 200 km over the ocean to a distance of 250 km over the ice sheet. The coastline is located at the ice-sheet margin. In order to ensure computational stability, it is assumed that 20 grid points near the inland lateral boundary have a flat topography.

The x direction in the model is prescribed to be 210°, which is considered to be that of the fall line. The topography is taken from Pettré et al. (1986). It may be assumed to be two-dimensional in the area of Dumont D'Urville, contrary to what is found near Mertz Glacier [e.g., Parish and Wendler (1991), their Fig. 4, p. 103]. When the terrain topography is not two-dimensional—for example, when a valley is present—the flow is enhanced on the left side of the valley (looking downward) but is weakened on its right side. The limited horizontal extent of such katabatic airflow will probably not favor the piling up of cold katabatic air when it slows down over the ocean. Furthermore, a return flow could exist on the right side of the valley in this case (Gallée 1996b, this issue). The rough homogeneity of the Adélie Land topography in the cross-slope direction allows the use of the two-dimensional version of MAR, with the horizontal axis parallel to the fall line. The horizontal grid spacing used in the simulations is 2 km. The main characteristics of the relevant stations and corresponding grid points are summarized in Table 1.

The vertical discretization consists of 30 levels irregularly spaced, with the finest discretization near the surface. Their initial heights above the ocean are 18 561, 16 721, 15 063, 13 570, 12 224, 11 011, 9917, 8930, 8038, 7231, 6496, 5823, 5200, 4611, 4040, 3468, 2880, 2274, 1675, 1136, 708, 410, 225, 118, 61, 31, 16, 8, 4, and 2 m.

The model is initialized using the procedure described in Gallée et al. (1995): the large-scale flow (u_L, v_L) is included by constraining its potential vorticity $E = (\zeta_L + f)/p_{*L}$ to remain constant, with $p_{*L} = p_{sL} - p_t$ being the large-scale pressure thickness and $\zeta_L = \partial v_L/\partial x - \partial u_L/\partial y$ being the large-scale vorticity. This is

done in particular to define the geostrophic wind, the initial wind, and the lateral boundary conditions for the wind from their values at D57.

3. Simulations

a. Initialization

Factors that could influence the evolution of the katabatic flow in the Adélie Land coastal zone are the diurnal cycle of insolation and the large-scale forcing.

Insolation is responsible for the surface heating, the subsequent weakening of the sloped inversion force, and the slowing down of the katabatic wind. Périard and Pettré (1993) have observed that a marked diurnal cycle in the Adélie Land wind is present during the summer period (October–February).

The impact of the large-scale wind forcing on the katabatic flow is also important. This has been mentioned and discussed by several authors, but up to now no complete explanation of this interaction has been proposed [see, e.g., Murphy and Simmonds (1993) for a review]. For example, Ball (1960) and Tauber (1960) suggest that strong winds occur when the large-scale wind component is from the same direction as the katabatic wind. Streten (1963) and Loewe (1974) found high wind speeds in association with below-average pressure, suggesting the presence of a low pressure system in the vicinity of the Antarctic continent. Pressure variations associated with a synoptic system moving in the vicinity of the Antarctic continent could also generate a gradient flow that reinforces or weakens the katabatic flow. Recently Bromwich et al. (1992) have found that a synoptic-scale pressure gradient favoring southerly geostrophic winds accelerates the southerly katabatic flow coming off the Ross Ice Shelf. Parish et al. (1993) suggest that strong katabatic winds over the Adélie Land ice-sheet margin are associated with low pressure over the coastal margin and easterly upper-level winds.

During summertime, the variations in the large-scale forcing may distort the daily cycle observed in Adélie Land. In this paper the impact of the large-scale forcing on the katabatic wind during summer is analyzed, with emphasis on the katabatic wind cessation.

The model is forced by the diurnal cycle of insolation of 1 December in Adélie Land (Fig. 1) for several large-scale situations. For each simulation, the large-scale forcing is fixed in time. A large-scale situation is characterized in the model by the large-scale wind and the initial vertical thermal structure of the atmosphere. It is further specified throughout the run through the lateral boundaries. The initial potential temperature sounding is modified by precluding potential temperature as smaller than the sea surface temperature. This is done to take into account maritime conditions prevailing in the Adélie Land coastal zone. In fact, the presence of a mixed layer is a characteristic of this area in summer [e.g., Parish et al. (1993), their Fig. 2.c].

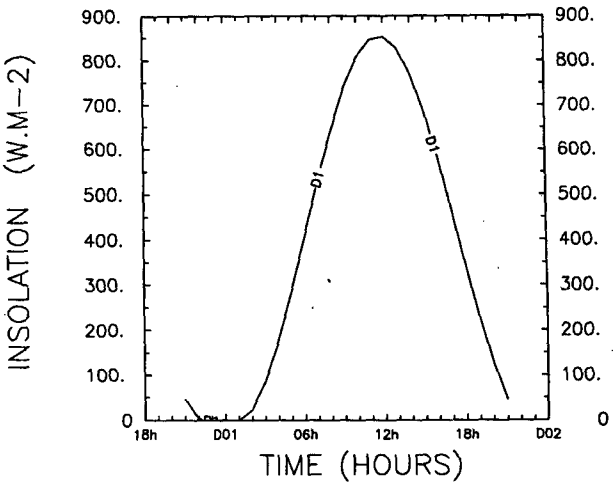

FIG. 1. The diurnal cycle of insolation for 1 December in Adélie Land.

Three soundings are taken into account. The first sounding, $\theta(z) = \max(271.2, 259 + 9z)$, where $\theta(z)$ is the potential temperature (K) and z is the altitude (km), corresponds to that of 3 December 1985, while the third, $\theta(z) = \max(271.2, 271 + 3z)$, corresponds to the November–December climatology of this region (see Parish et al. 1993). The soundings have been chosen in order to give the same potential temperature 2 km above the mean sea level. The large-scale wind speed is assumed to be 10 m s^{-1} at D57.

The simulations are started at 0900 LT and are conducted over 36 h. The model needs roughly a 12-h time integration before the circulation is well established. For this reason, only the last 24 h of the integration are considered.

b. Impact of the atmospheric thermal structure

The atmospheric thermal structure may influence the distribution of the longwave radiative heat flux. For example, lower atmospheric temperatures above the katabatic layer are responsible for a lower downward longwave radiative flux and a subsequent increase of the negative buoyancy. In order to examine the impact of this process over the rather steep slopes of Adélie Land, the sensitivity to the three atmospheric soundings is analyzed in experiments with zero large-scale wind. During the night, the surface cooling is due to net longwave radiative heat losses. Nevertheless, the atmosphere itself is not significantly affected by the longwave radiative flux but rather by the flux of sensible heat from the atmosphere to the colder surface. In fact, the divergence of the latter across the katabatic layer is generally larger than the former by one order of magnitude.

It is found that at D47 during nighttime, the net longwave heat losses from the surface amount to 55 and 45

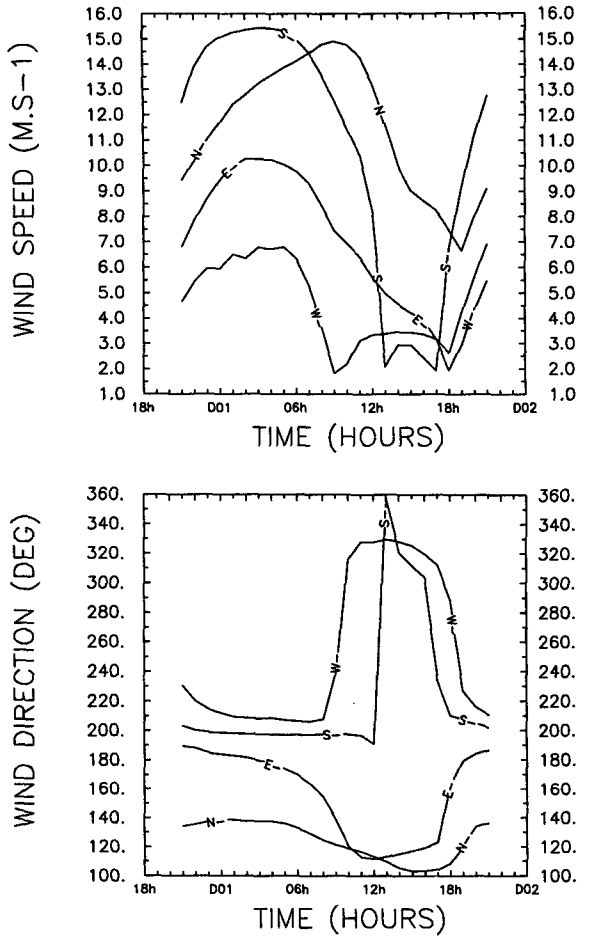

FIG. 2. The simulated diurnal cycle of (a) the wind speed and (b) the wind direction at D10. The large-scale wind speed at D57 is 10 m s^{-1}. Lines labeled by N, E, S, and W correspond to the large-scale wind direction at D57 from 30°, 120°, 210°, and 300°. The initial potential temperature vertical profile is $\theta(z) = \max(271.2, 271 + 3z)$, where z is in kilometers.

W m^{-2} for $\theta(z) = \max(271.2, 271 + 3z)$ and $\theta(z) = \max(271.2, 259 + 9z)$, respectively, while the sensible heat losses from the atmosphere amount to 15 and 10 W m^{-2} and the katabatic wind speeds amount to 6 and 4.5 m s^{-1}. The larger net longwave radiative heat losses when $\theta(z) = \max(271.2, 271 + 3z)$ may be related to a colder atmosphere above 2 km. The smaller sensitivity found in the sensible heat flux may be due to the stronger atmospheric stability near the colder surface, when the net longwave radiative heat losses are larger. The sensitivity found in the katabatic wind speed is slightly larger than that found by Ye et al. (1990). Using both an analytical and a modeling approach, these authors found a downslope flow relatively insensitive to the atmospheric sounding and suggest that the thermal structure of the katabatic layer has a larger influence on the katabatic wind speed than the background atmospheric thermal profile.

A comparable sensitivity is found for a nonzero large-scale wind.

c. *Impact of the large-scale wind direction*

In Table 2, the simulated downslope (katabatic) wind component (from the 210° direction) is shown for four directions of the large-scale wind and the three large-scale air stratifications. The results shown are those at D10—that is, on the steepest slope, 5 km from the ice-sheet margin (see Table 1). They are taken 2 m above the surface at midnight.

At this time of the day, the strongest downslope winds are simulated when the large-scale wind is downslope and the weakest when it is in the upslope direction. Nevertheless, in this case the katabatic flow is in the opposite direction of the large-scale flow. This behavior may be related to the strong inversion above the katabatic layer. Van den Broeke and Bintanja (1995) have shown that in this case the surface flow must have a downslope component.

Intermediate values of the downslope wind speed are found when the large-scale wind is in the cross-slope direction, but these values are larger when the large-scale wind is from 120°. This corresponds to a large-scale high pressure system over the continent or a low pressure system off the coast and is referred to as an easterly wind. In this case the relatively small contribution from the large-scale wind to the surface wind through Ekman pumping is from the continent. The efficiency of this process is slightly increased for the weakest background stability, probably in conjunction with an enhancement of turbulence in this case. Note that the difference of the model response to easterly and westerly large-scale winds is in qualitative agreement with the climatology of this region (Parish et al. 1993).

The variations in time of the wind speed and direction at D10 are shown in Fig. 2 for the wind speed and directions mentioned in Table 2 and for the weakest background stability. A steady-state diurnal cycle is simulated. It is well marked, in agreement with the climatology (e.g., Périard and Pettré 1993). During nighttime, katabatic conditions are simulated in all experiments. During daytime, a stronger turbulent mixing oc-

TABLE 2. Simulations of katabatic wind in Adélie Land. Simulated downslope wind component (m s^{-1}), 2 m above the surface, for D10 and at midnight (i.e., after 15-h simulation). The large-scale wind speed is 10 m s^{-1} at D57. The initial potential temperature profile $\theta(z)$ (K) is characterized by its mean sea level value and its gradient (K km^{-1}); z is given in kilometers.

	Large-scale wind direction			
$\theta(z)$	30°	120°	210°	300°
max(271.2, 259 + 9z)	3.2	7.7	14.2	6.5
max(271.2, 265 + 6z)	3.6	7.9	14.8	6.7
max(271.2, 271 + 3z)	3.8	8.5	14.8	5.9

TABLE 3. Simulations of katabatic wind in Adélie Land. Sensitivity to the large-scale forcing. Simulated downslope wind component (m s^{-1}), 2 m above the surface, for D10 and at midnight (i.e., after 15-h simulation). The large-scale wind direction at D57 is that of the fall line (210°). The initial potential temperature profile $\theta(z)$ (K) is characterized by its mean sea level value and its gradient (K km^{-1}); z is given in kilometers.

	Large-scale wind speed (m s^{-1})				
$\theta(z)$	0	5	10	15	20
max(271.2, 259 + 9z)	7.3	5.6	14.2	15.7	14.7
max(271.2, 265 + 6z)	7.4	8.0	14.8	16.1	16.0
max(271.2, 271 + 3z)	7.4	10.9	14.8	15.8	16.8

curs in the boundary layer. Therefore, the atmospheric circulation in the boundary layer could be more markedly influenced by the large-scale wind. This influence may be seen in the simulated wind direction (Fig. 2) when the large-scale wind is from 120° (easterly wind) or 300° (westerly wind).

When the large-scale wind is from 30° (upslope wind) or 210° (downslope wind), the resulting atmospheric circulation is more complex. In the former case, a strong horizontal temperature gradient results from the counteraction of the cold katabatic air descending the ice sheet and the warm air advected from the ocean by the upslope large-scale wind. In the Southern Hemisphere, the associated strong thermal wind is from west to east in this case. Since the cross-slope component of the large-scale wind is zero, an easterly barrier wind is generated in the lower troposphere. Comparable situations are described for the Antarctic Peninsula by Parish (1983) and for the Greenland ice sheet by Meesters (1994). Note that the wind increase during daytime (Fig. 2) reflects the penetration of the barrier wind in the boundary layer.

Concerning the latter case (i.e., when the large-scale wind is downslope), further analysis of Fig. 2 indicates that the model simulates a decrease of the katabatic wind larger than 10 m s^{-1} in less than 1 h 30 min, just after 1200 LT. In fact, the large-scale wind in the lower troposphere at D57 was also downslope on 3 December 1985. Since the main interest of this paper is a better understanding of the processes governing the sudden katabatic wind cessation, the next experiments will be restricted to a large-scale wind forcing from this direction.

d. Impact of the large-scale wind speed

Table 3 shows the sensitivity of the simulated downslope wind component to the large-scale wind speed when it is in the downslope direction at D57. The results shown are those from D10, 2 m above the surface at midnight. When the large-scale air stability is moderate (i.e., $\partial\theta/\partial z$ = 3 K km^{-1}), the downslope wind component increases with the large-scale wind speed. A more complex sensitivity is found when the large-scale air stability is strong (i.e., $\partial\theta/\partial z$ = 9 K km^{-1}). This could be due to the formation of an unstable katabatic layer aloft, which is responsible for a horizontal temperature gradient and a pressure gradient force in the opposite direction to the katabatic wind. The unstable layer development is more marked for a stabler initial air stratification and stronger downslope wind speeds. The subsequent return flow aloft precludes the direct influence of the large-scale wind on the katabatic flow. Further explanation about the behavior of the unstable layer is given below.

Analyzing the results in more detail, it is found that the katabatic wind speed decrease at D10, when the large-scale (downslope) wind speed increases from zero to 5 m s^{-1} (Table 3), is significant. In fact, the katabatic wind maximum is larger when the large-scale wind speed is 5 m s^{-1} but is simulated further upslope (Fig. 3). The apparent decrease results from the slowing down of the katabatic flow before it reaches D10, probably because of the generation of the unstable katabatic layer over the steep slopes.

e. Katabatic wind cessation

Table 4 shows the variation of the downslope wind component u during the katabatic wind cessation. A time t_J is defined as the time t > 0000 LT of the maximum decrease of u within 10 min (i.e., $\partial u/\partial t$, with δt = 10 min). Since the decrease of u starts well before $t = t_J$ and ends well after, a more complete description of the variation of u during the wind cessation at D10 is given by

$$\Delta u = u(\text{D10}, t_J + 30\ \text{min}) - u(\text{D10}, t_J - 1\ \text{h}).$$

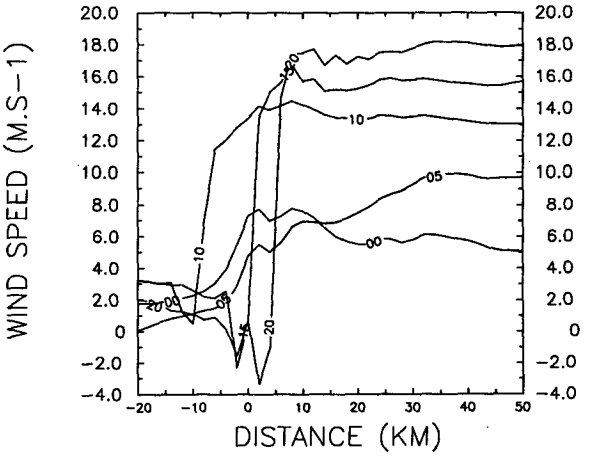

FIG. 3. The simulated downslope component of the wind, 2 m above the surface and at 0000 LT, when the direction of the large-scale wind at D57 is downslope. Lines labeled by 0, 5, 10, 15, and 20 correspond to the large-scale wind speed at D57, amounting, respectively, to 0, 5, 10, 15, and 20 m s^{-1}. The initial potential temperature vertical profile is $\theta(z)$ = max(271.2, 259 + 9z), where z is in kilometers.

TABLE 4. Simulations of katabatic wind in Adélie Land. Sensitivity to the large-scale forcing. Simulated variation (m s^{-1}) of the downslope wind component after midnight at D10 2 m above the surface. (The time of occurrence is indicated in parentheses). The large-scale wind direction at D57 is that of the fall line (210°). The initial potential temperature profile $\theta(z)$ (K) is characterized by its mean sea level value and its gradient (K km^{-1}); z is given in kilometers.

	Large-scale wind speed (m s^{-1})				
$\theta(z)$	0	5	10	15	20
max(271.2, 259 + 9z)	−3.8 (0900)	−5.4 (0900)	−12.5 (0940)	−17.7 (0450)	−20.9 (0040)
max(271.2, 265 + 6z)	−3.6 (0850)	−5.9 (0950)	−13.2 (1040)	−18.1 (0820)	−17.3 (0200)
max(271.2, 271 + 3z)	−3.9 (0950)	−5.8 (1110)	−10.6 (1220)	−12.4 (1100)	−18.5 (0330)

In Table 4, negative values indicate a decrease of the katabatic wind speed. The time of occurrence t_J is indicated between brackets. The magnitude of the variation is comparable to that of the large-scale wind forcing at D57. Except in the case of no large-scale wind forcing, this variation corresponds to a change from downslope to upslope wind conditions.

A surface pressure variation $\Delta p(x, t_J)$ (hereafter referred to as the pressure transition) may be associated with the maximum wind decrease $\Delta u(x, t_J)$. It is computed from the surface pressure $p'(x, t)$, corrected as follows from the altitude effect and the domain-averaged surface pressure variations in time:

$$p'(x, t) = p_s(x, t) - p_s(x_0, t) - [p_s(x, t_0) - p_s(x_0, t_0)], \quad (2)$$

where t is time, t_0 is the initial time, x is the distance of the considered grid point from the ice-sheet margin, and x_0 is the distance of a reference grid point over the ocean from the ice-sheet margin (not influenced by the katabatic wind cessation). We have chosen $x_0 = -20$ km. Table 5 presents the pressure transition

$$\Delta p \text{ (hPa)} = p'(\text{D10}, t_J + 30 \text{ min}) - p'(\text{D10}, t_J - 1 \text{ h})$$

at D10. It is found that the pressure transition is larger than 0.5 hPa for large-scale wind speeds equal to or stronger than 10 m s^{-1}. In this case, the variation of the downslope wind component simulated by MAR has some aspects in common with the Loewe's phenomenon.

The location of the katabatic wind cessation over the ice sheet is modulated by the diurnal cycle of insolation. Upslope wind conditions develop in the morning and start at the ice-sheet margin. A maximum advance in the ice-sheet interior is simulated in the afternoon, amounting to a few tens of kilometers. A detailed comparison of the experiments show that this maximum advance is a function of the large-scale wind speed. When the large-scale wind is weak (i.e., $\leq$5 m s^{-1} at D57), the maximum advance is rather important (more than 50 km). In this case, the upslope wind results from a positive buoyant force along the slope and is anabatic.

When the large-scale wind speed is strong (i.e., $\geq$15 m s^{-1} at D57), the maximum advance decreases down to roughly 10 km. Furthermore, the propagation of the simulated katabatic airflow over the ocean is reduced for increased large-scale wind from 210° and does not reach the coastal weather station DDU (Dumont d'Urville) for a wind forcing in excess of 10 m s^{-1}. Such behavior of the model could perhaps explain why some previous studies based on observations in the Antarctic coastal zone do not mention the occurrence of strong katabatic flows in conjunction with strong offshore large-scale winds.

f. The standard simulation

1) COMPARISON WITH THE OBSERVATIONS

The case corresponding to a large-scale forcing of 15 m s^{-1} (from 210°) and $\theta(z)$ = max(271.2, 259 + 9z) comes close to the situation of 3 December 1985. It is referred to hereafter as the standard experiment. Figure 4 presents the simulated evolution at D10 of the 2-m-high downslope wind component and temperature, and the corrected surface pressure $p'(x, t)$. The model output is taken every 10 min and shows a rather sudden character of the transition between downslope and upslope wind conditions, as it would appear to a static observer. Figure 4 may be compared to Fig. 3 of Pettré and André (1991). Taking into account the idealized large-scale forcing assumed in the model, general agreement is found. The wind transition occurs in about 20 min at roughly 0630 LT in the observations and in about 90 min at 0450 LT in the simulation. The differences in the duration of the transition between simulation and observation could be due to the coarse hor-

TABLE 5. Simulations of katabatic wind in Adélie Land. Sensitivity to the large-scale forcing. Simulated surface pressure variation (hPa) after midnight at D10. (The time of occurrence is indicated in parentheses.) The large-scale wind direction at D57 is that of the fall line (210°). The initial potential temperature profile $\theta(z)$ (K) is characterized by its mean sea level value and its gradient (K km^{-1}); z is given in kilometers.

	Large-scale wind speed (m s^{-1})				
$\theta(z)$	0	5	10	15	20
max(271.2, 259 + 9z)	0.03 (0900)	0.06 (0900)	1.06 (0940)	2.19 (0450)	2.71 (0040)
max(271.2, 265 + 6z)	0.02 (0850)	0.08 (0950)	1.17 (1040)	2.20 (0820)	2.31 (0200)
max(271.2, 271 + 3z)	0.05 (0950)	0.05 (1110)	0.72 (1220)	1.36 (1100)	2.55 (0330)

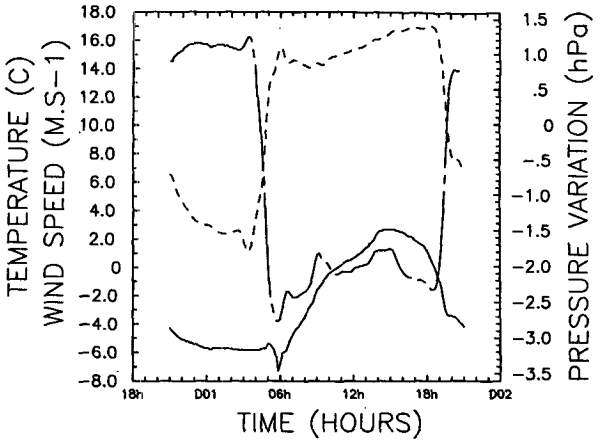

FIG. 4. Simulated evolution of the 2-m-high downslope wind component (dash–dotted line) and temperature (solid line), and the surface pressure (dashed line) at D10 for the standard experiment. The model output is taken every 10 min.

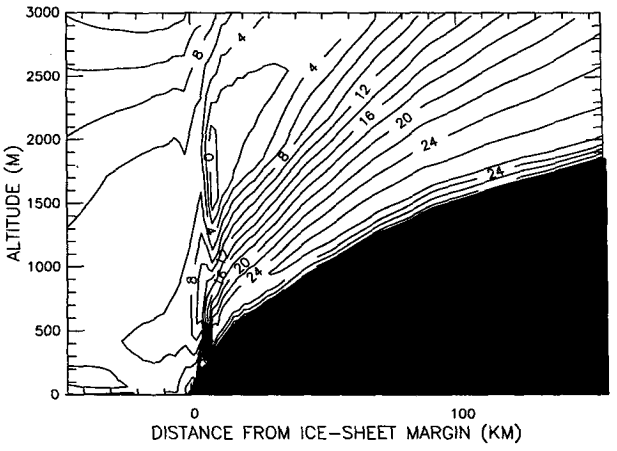

FIG. 5. The x (downslope) component of the wind field in the vertical plane of integration for the standard experiment, after 20-h time integration (i.e., at 0500 LT), as a function of distance to the ice-sheet margin (positive distances are on the ice sheet) and height above the surface. Positive values indicate downslope wind and are represented by solid lines. The contour interval is 2 m s^{-1}.

izontal grid spacing used in the model, while the actual horizontal scale of the Loewe's phenomenon is much smaller. The simulated pressure transition (2.2 hPa) is smaller than the observed pressure jump (5.5 hPa). This difference is significant, indicating that the model probably does not simulate the Loewe's phenomenon itself. However, the simulation of a surface pressure transition in the hydrostatic model suggests the possible role of hydrostatic processes in the causes of a Loewe's phenomenon. In fact, the horizontal wavelength of the simulated transition may be assumed to be twice the grid spacing, or 4 km, and the vertical extent is about 2 km (see Fig. 7). After Pielke (1984), the ratio 0.03 L_z^2/L_x^2 should be much less than 1 in order to neglect the nonhydrostatic effects. In our simulated case, this ratio is 0.0075, showing that our model can simulate the hydrostatic part of the Loewe's phenomenon and that the main forcing cause of it is hydrostatic. The actual observed Loewe's phenomenon has a shorter horizontal wavelength. Furthermore, it is accompanied by a wall of drifting snow and clouds just above, revealing vertical acceleration. It is thus nonhydrostatic and cannot be simulated by the model. It is possible that the vertical deceleration of the downslope flow just in front of a jump could enhance the vertical pressure gradient and subsequently contribute to the observed large pressure contrast across the jump. In order to understand fully the jump itself, some nonhydrostatic runs must be done, but this will require the use of a nonhydrostatic model, which must still be developed.

Let us now consider in more detail the main simulated variables. Figures 5, 6, and 7 show, respectively, the downslope wind component, the cross-slope wind component, and the potential temperature for the standard simulation at 0500 LT (i.e., after 20-h time integration) in the vertical plane of integration. The simulation of the cross-slope wind component is in qualitative agreement with the observations (see Fig. 5 of Pettré and André 1991). (i) Upstream of the wind cessation, it exhibits significantly smaller values than the downslope wind component in agreement with the essentially downslope character of the katabatic wind. (ii) An easterly wind component is found downstream of the wind cessation at low levels and probably results from the thermal wind balance between a pool of cold air just in front of the wind cessation and relatively warmer air out to sea (see Fig. 7). This pool of cold

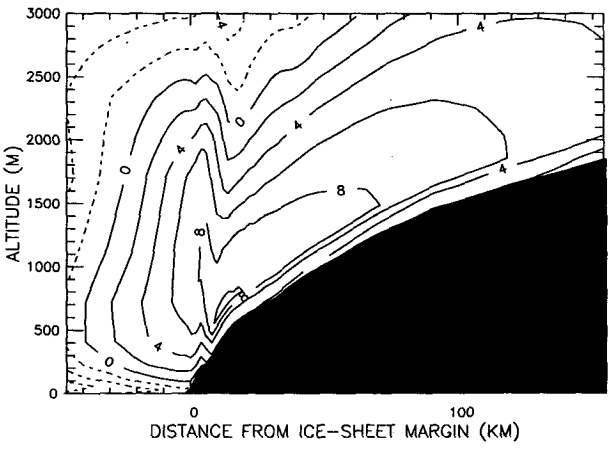

FIG. 6. The y (cross-slope) component of the wind field in the vertical plane of integration for the standard experiment, after 20-h time integration (i.e., at 0500 LT), as a function of distance to the ice-sheet margin (positive distances are on the ice sheet) and height above the surface. Positive values indicate a cross-slope component from the 120° direction and are represented by solid lines. The contour interval is 2 m s^{-1}.

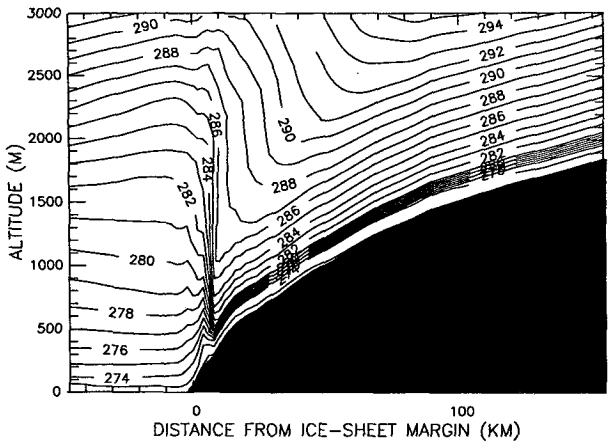

FIG. 7. The potential temperature in the vertical plane of integration for the standard experiment, after 20-h time integration (i.e., at 0500 LT), as a function of distance to the ice-sheet margin (positive distances are on the ice sheet) and altitude. The contour interval is 2 K.

air is generated by the piling up of cold air in front of the katabatic airflow, as explained below.

Figure 5 shows the katabatic wind cessation occurring near the ice-sheet margin, while the analysis of Fig. 7 also allows more insight into the causes of the katabatic wind cessation and the associated pressure transition. A sharp discontinuity is found in this figure between the potential temperature field upstream and downstream of the pressure transition. For upstream conditions, the model simulates the thermodynamic structure of the katabatic layer observed during the IAGO campaign (Pettré and André 1991). From the surface upward, it consists of a nearly neutral layer capped by a strong inversion, which, over the steep slopes, is topped by a deep unstable layer capped by a stable transition layer to the free atmosphere. The observations made during the IAGO campaign also show that the nearly neutral katabatic layer does not thicken over the steep slopes of Adélie Land and that the thickness of the inversion is comparable to that of the nearly neutral layer. This behavior is also a characteristic of the simulation, as may be seen in Fig. 7.

2) THE UNSTABLE LAYER

The formation of the unstable layer results from detrainment in the katabatic layer under moderate or strong downslope wind conditions when the initial large-scale stratification is stable. In this case, the adiabatic warming of the air parcels coming from the high ice-sheet interior is such that these air parcels become warmer than those of the more quiescent environment. For increasing downslope wind speed, the turbulent mixing bringing cold air from the surface through the inversion becomes less rapid than the adiabatic warming. The possibility for detrainment to exist is also mentioned in Lalaurette and André (1985), who used an integral model of katabatic flow. Unfortunately, this process is not taken into account in integral models.

It should also be mentioned that an unstable layer has been observed during the Greenland Ice Margin Experiment (GIMEX) campaign over the Greenland ice sheet (van den Broeke et al. 1994, their Fig. 9) and simulated with MAR (Gallée et al. 1995, their Fig. 12). Nevertheless, the environmental conditions were different in that area because of the presence of a warm tundra near the ice-sheet margin. It is possible that the unstable layer in that area is a result of surface heating over the Greenland tundra (van den Broeke et al. 1994), although the piling up of relatively cold stable katabatic air also seems to occur over the tundra during daytime, inhibiting the formation of a deep mixed layer just at the ice-sheet margin (Gallée et al. 1995).

A consequence of the adiabatic warming is that relatively warm air is found at low levels near the ice-sheet margin. Downstream of the wind cessation, more quiescent conditions prevail and the air is colder. This horizontal temperature difference is responsible for a surface pressure difference between the two air masses.

3) THE PILING UP OF COLD AIR

Another important process contributes to the pressure transition in front of the katabatic airstream. Indeed, cold air that has formed in the nearly neutral katabatic layer piles up in front of the katabatic airstream because of the strong slowing down of the wind in this area. This effect reinforces the contrast between a colder quiescent lower troposphere downstream and a warmer one upstream. The temperature contrast in front of the katabatic airstream partly explains the pressure contrast and the subsequent strong slowing down of the katabatic flow. In other words, the accumulation of cold air over the ocean acts as a positive feedback and is responsible for the sharpening of the front between the two air masses.

It should be mentioned that the piling up of cold air was also found for the night situation during GIMEX, leading to a strong slowing down of the wind over the tundra at this time (van den Broeke et al. 1994; Gallée et al. 1995).

4) COMPARISON WITH BALL'S THEORY

The results of the standard experiment could also be analyzed in light of the theory of Ball (1956). Nevertheless, such analysis must be done carefully because the characteristics of the simulated katabatic flow are not strictly comparable to those of the ideal katabatic flow assumed by Ball (1956). For example, the thickness of the simulated inversion and the nearly neutral layer are comparable, while in the Ball (1956) model it is not. Furthermore, the progressive detrainment from the inversion top is not taken into account (Lalaurette and André 1985). Finally, downstream of a jump, the

simple Ball (1956) hypothesis of a constant mass flux probably does not hold since piling up occurs. Taking that in mind, a Froude number is defined as

$$F = U\left[g\left(\frac{\Delta\bar{\theta}}{\theta_0}\right)h \right]^{-1/2},$$

where h is the depth of the katabatic layer, chosen as the height at which the downslope component of the simulated wind becomes smaller than that of the large-scale wind. Since a return flow is simulated in the unstable katabatic sublayer, this choice of h allows easy exclusion of this sublayer. Another reason for this choice of h is that its determination from the potential temperature field is a potential source of error because of the complex thermal structure of the katabatic layer. Finally, a consequence of this choice is that the Froude number must be set equal to zero where upslope flow prevails near the surface. Of the remaining variables in the equation above, U and $\Delta\bar{\theta}$ are, respectively, the downslope wind component and the potential temperature deficit averaged over h, and θ_0 is the potential temperature above the inversion.

The diurnal cycle of the Froude number is shown in Fig. 8 for the standard experiment. The sensible and net longwave radiative heat fluxes at the surface are also shown. In order to allow easier comparison, the longwave radiative heat flux is negative when downward.

A well-marked diurnal cycle may be seen. The Froude number is supercritical (i.e., larger than 1) or zero. The transition between supercritical values and zero is abrupt, in qualitative agreement with the Ball (1956) theory, and occurs at the same time as the katabatic wind cessation simulated by the model. An increase of the kabatic layer depth is simulated just before the katabatic cessation. It corresponds to an increase of the turbulent kinetic energy in the katabatic layer in conjunction with increasing surface heating. Note that when the depth of the katabatic layer is computed from the potential temperature field, an abrupt transition from supercritical values to zero is also found at the same time.

Comparing the longwave radiative heat losses by the surface to the sensible heat losses by the atmosphere, it is seen that during nighttime the latter are stronger by roughly 40 W m^{-2}. Neglecting the relatively small contribution from the subsurface heat flux, this additional surface warming may be correlated to an additional cooling due to an important sublimation into the dry katabatic air. It is possible that the resulting additional atmospheric cooling helps the katabatic wind to be maintained against the strong adiabatic warming over the steepest slopes.

During daytime, the sensible heat flux is very small and the sublimation is reduced by at least 50%. The surface energy balance is influenced mainly by the absorbed solar radiation (up to 170 W m^{-2}) and the longwave radiative heat losses.

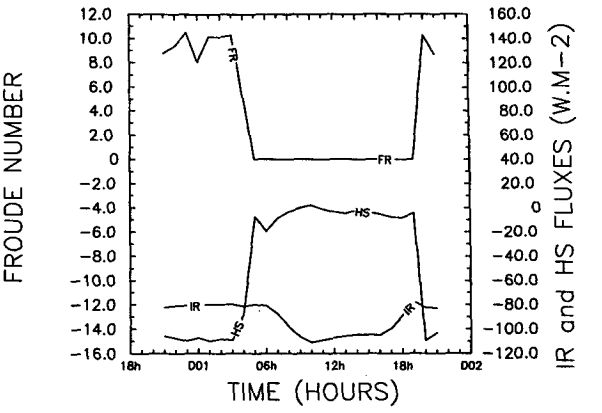

FIG. 8. Diurnal cycle of the Froude number (labeled FR), and the sensible (labeled HS, negative downward) and net longwave radiative (labeled IR, positive downward) heat fluxes at the surface for the standard experiment.

It is also found that the sensible heat flux starts to decrease roughly 1 h before the katabatic wind cessation. Consequently, the atmospheric cooling and the negative buoyancy are reduced. This suggests that the dynamical balance of the katabatic airflow is constrained by the sensible heat flux. Indeed, the inversion strength of the katabatic layer is reinforced by the turbulent cooling from below but destroyed by adiabatic warming and subsequent detrainment of the air parcels from its top. This process is particularly efficient after a long descent—that is, near the ice-sheet margin. When insolation increases during the morning, the surface warming reduces the downward sensible heat flux. Consequently, the turbulent cooling of the katabatic layer is smaller, and the dynamical stability of the katabatic layer is reduced in this area.

5) SUMMARY

The main steps characterizing the generation of a katabatic wind cessation in the standard simulation could then be summarized as follows.

1) A piling up of cold katabatic air out to sea results from a dissipation of the negative buoyant force in this area.

2) The pressure gradient force associated with this piling up amplifies the initial deceleration and piling up of the katabatic air and subsequently causes wind cessation somewhere in the coastal area.

3) The pressure difference in front of the katabatic airstream is sharpened because of the significant thermal contrast between the adiabatically warmed unstable layer upstream and the piled-up cold air downstream of the katabatic cessation.

4) When, in the morning, the increase of the insolation causes a decrease of the negative buoyant force

responsible for the katabatic flow, the cold air accumulated over the coastal area spreads toward the ice sheet and the pressure transition in front of it moves upslope.

4. Conclusions

The purpose of the present paper is to examine the possible influence of the large-scale forcing on the katabatic wind cessation and the associated surface pressure transition, which are often observed in the Antarctic coastal zone. The mesoscale model MAR has been forced by the diurnal cycle of insolation corresponding to early summer in Adélie Land (Antarctica). Situations with a downslope large-scale wind forcing are analyzed in detail. In this case, downslope (katabatic) winds are simulated during the night. During daytime, upslope wind conditions may develop over the steepest slopes, starting from the ice-sheet foot and having a maximum extent of up to a few tens of kilometers in the mid afternoon. The change from downslope to upslope wind conditions occurs roughly over ten kilometers and appears to be sudden to a static observer.

When the downslope large-scale winds are moderate or strong, the simulated amplitude of the wind transition is larger. In particular, the large-scale situation chosen for one of the simulations presented in this paper comes very close to that observed on 3 December 1985 by Pettré and André (1991). In this case, the model simulates a wind cessation and a pressure transition. This behavior has some aspects in common with the Loewe's phenomenon observed on this date.

The physical mechanism responsible for the 3 December 1985 katabatic wind cessation simulated by the model is linked to strong, downslope-directed large-scale winds. These are responsible for the formation of a deep unstable layer over the ice-sheet margin and the piling up of cold air in front of the katabatic airstream. A pressure gradient force is generated in the unstable layer and is directed toward the ice-sheet interior. It slows down the flow in the upper part of the katabatic layer and is even responsible for a return flow aloft. The piling up of cold air amplifies the katabatic wind cessation. It may be viewed as a positive feedback. Both processes are responsible for the generation of a significant surface pressure transition in front of the katabatic flow.

This suggests that hydrostatic processes may be at least partly responsible for the occurrence of a Loewe's phenomenon. However, the Loewe's phenomenon itself has a very small horizontal scale and is probably characterized by strong vertical accelerations. Consequently, a full understanding of it will require that nonhydrostatic processes and a very small horizontal grid size be taken into account.

Acknowledgments. This research is sponsored by the Belgian program Scientific Research on the Antarctic (Services of the Prime Minister—Federal Office for Scientific, Technical and Cultural Affairs) under Contract A3/10/001. The authors wish to thank Dr. Brad Murphy and Dr. Peter Duynkerke for their suggestions, and Prof. André Berger and Dr. Jean-Pascal van Ypersele for continued support.

REFERENCES

Alpert, P., A. Cohen, J. Neumann, and E. Doron, 1982: A model simulation of the summer circulation from the eastern Mediterranean past Lake Kinneret in the Jordan Valley. *Mon. Wea. Rev.*, **110,** 994–1006.

Anthes, R. A., Y.-H. Kuo, E.-Y. Hsie, S. Low-Nam, and T. W. Bettge, 1989: Estimation of skill and uncertainty in regional numerical models. *Quart. J. Roy. Meteor. Soc.*, **115,** 763–806.

Ball, F. K., 1956: The theory of strong katabatic winds. *Aust. J. Phys.*, **9,** 373–386.

——, 1960: Winds on the ice slopes of Antarctica. *Antarctic Meteorology,* Pergamon Press, 9–16.

Bromwich, D. H., J. F. Carrasco, and C. R. Stearns, 1992: Satellite observations of katabatic wind propagation for great distances across the Ross Ice Shelf. *Mon. Wea. Rev.*, **120,** 1940–1949.

Deardorff, J. W., 1978: Efficient prediction of ground surface temperature and moisture with inclusion of a layer of vegetation. *J. Geophys. Res.*, **83,** 1889–1903.

Duynkerke, P. G., 1988: Application of the $E-\epsilon$ turbulence closure model to the neutral and stable atmospheric boundary layer. *J. Atmos. Sci.*, **45,** 865–880.

Gallée, H., 1995: Simulation of the mesocyclonic activity in the Ross Sea, Antarctica. *Mon. Wea. Rev.*, **123,** 2051–2069.

——, 1996: Mesoscale atmospheric circulations over the southwestern Ross Sea sector, Antarctica. *J. Appl. Meteor.*, **35,** 1129–1141.

——, and G. Schayes, 1992: Dynamical aspects of katabatic winds evolution in the Antarctic coastal zone. *Bound.-Layer Meteor.*, **59,** 141–161.

——, and ——, 1994: Development of a three-dimensional meso-γ primitive equations model, katabatic winds simulation in the area of Terra Nova Bay, Antarctica. *Mon. Wea. Rev.*, **122,** 671–685.

——, J. P. van Ypersele, T. Fichefet, C. Tricot, and A. Berger, 1991: Simulation of the last glacial cycle by a coupled 2D climate–ice sheet model. Part 1: The climate model. *J. Geophys. Res.*, **96,** 13 139–13 161.

——, O. Fontaine de Ghélin, and M. van den Broeke, 1995: Simulation of atmospheric circulation during the GIMEX 91 experiment using a meso-γ primitive equations model. *J. Climate,* **8,** 2843–2859.

Klemp, J. B., and D. K. Lilly, 1978: Numerical simulation of hydrostatic waves. *J. Atmos. Sci.*, **35,** 78–107.

Lalaurette, F., and J.-C. André, 1985: On the integral modeling of katabatic flows. *Bound.-Layer Meteor.*, **33,** 135–149.

Lied, N. T., 1964: Stationary hydraulic jumps in a katabatic flow near Davis, Antarctica. *Aust. Meteor. Mag.*, **47,** 40–51.

Loewe, F., 1974: Considerations concerning the winds of Adélie Land. *Z. Gletscherkunde Glazialgeologie,* **10,** 189–197.

Mather, K. B., and G. S. Miller, 1967: Notes on topographic factors affecting the surface wind in Antarctica, with special reference to katabatic winds, and bibliography. Tech. Rep. of the University of Alaska, Grant GA 900, 63 pp.

Meesters, A., 1994: Dependence of the energy balance of the Greenland ice sheet on climate change: Influence of katabatic wind and tundra. *Quart. J. Roy. Meteor. Soc.*, **120,** 491–518.

Morcrette, J. J., 1984: Sur la paramétrisation du rayonnement dans les modèles de la circulation générale atmosphérique. Ph.D. thesis, University of Science and Technology at Lille, 373 pp.

Murphy, B. F., and I. Simmonds, 1993: An analysis of strong wind events in a GCM near Casey in the Antarctic. *Mon. Wea. Rev.*, **121,** 522–534.

Parish, T. R., 1983: The influence of the Antarctic Peninsula on the wind field over the western Weddell Sea. *J. Geophys. Res.,* **88,** 2684–2692.

——, and G. Wendler, 1991: The katabatic wind regime at Adélie Land, Antarctica. *Int. J. Climatol.,* **11,** 97–107.

——, P. Pettré, and G. Wendler, 1993: The influence of large-scale forcing on the katabatic wind regime at Adeélie Land, Antarctica. *Meteor. Atmos. Phys.,* **51,** 165–176.

Périard, C., and P. Pettré, 1993: Some aspects of the climatology of Dumont d'Urville. *Int. J. Climatol.,* **13,** 313–327.

Pettré, P., and J.-C. André, 1991: Surface-pressure change through Loewe's phenomena and katabatic flow jumps: Study of two cases in Adélie Land, Antarctica. *J. Atmos. Sci.,* **48,** 557–571.

——, J. F. Pinglot, M. Pourchet, and L. Reynaud, 1986: Accumulation distribution in Terre Adélie, Antarctica: Effect of meteorological parameters. *J. Glaciol.,* **32,** 486–500.

Pielke, R. A., 1984: *Mesoscale Meteorological Modeling.* Academic Press, 612 pp.

Schwerdtfeger, W., 1984: *Weather and Climate of the Antarctic.* Vol. 15, *Developments in Atmospheric Sciences,* Elsevier, 261 pp.

Segal, M., J. R. Garratt, R. A. Pielke, and Z. Ye, 1991: Scaling and numerical model evaluation of snow-cover effects on the generation and modification of daytime mesoscale circulations. *J. Atmos. Sci.,* **48,** 1024–1042.

Streten, N. A., 1963: Some observations of Antarctic katabatic winds. *Aust. Meteor. Mag.,* **42,** 1–23.

Tauber, G. M., 1960: Characteristics of Antarctic katabatic winds. *Antarctic Meteorology,* Pergamon Press, 52–64.

Tricot, C., and A. Berger, 1988: Sensitivity of present-day climate to astronomical forcing. *Long and Short Term Variability of Climate Lecture Notes Earth Sci.,* Vol. 16, H. Wanner and U. Siegenthaler, Eds., Springer Verlag, 132–152.

——, P. G. Duynkerke, and J. Oerlemans, 1994: The observed katabatic flow at the edge of the Greenland ice sheet during GIMEX-91. *Global Planet. Change,* **9,** 3–15.

van den Broeke, M. R., and R. Bintanja, 1995: Summertime atmospheric circulation in the vicinity of a blue ice area in Queen Maud Land, Antarctica. *Bound.-Layer Meteor.,* **72,** 411–438.

Ye, Z. J., J. R. Garratt, M. Segal, and R. A. Pielke, 1990: On the impact of atmospheric thermal stability on the characteristics of nocturnal downslope flows. *Bound.-Layer Meteor.,* **51,** 77–97.